ResearchGate

See discussions, stats, and author profiles for this publication at: https://www.researchgate.net/publication/49764146

Development of Ultrabright Semiconducting Polymer Dots for Ratiometric pH Sensing

ARTICLE *in* ANALYTICAL CHEMISTRY · FEBRUARY 2011

Impact Factor: 5.64 · DOI: 10.1021/ac103140x · Source: PubMed

CITATIONS
95

READS
45

6 AUTHORS, INCLUDING:

Yang-Hsiang Chan
National Sun Yat-sen University
30 PUBLICATIONS **849** CITATIONS
SEE PROFILE

Fangmao Ye
University of Washington Seattle
30 PUBLICATIONS **726** CITATIONS
SEE PROFILE

Yuhui Jin
University of Washington Seattle
26 PUBLICATIONS **1,171** CITATIONS
SEE PROFILE

Available from: Yang-Hsiang Chan
Retrieved on: 02 February 2016

NIH Public Access
Author Manuscript
Anal Chem. Author manuscript; available in PMC 2012 February 15.

Published in final edited form as:
Anal Chem. 2011 February 15; 83(4): 1448–1455. doi:10.1021/ac103140x.

Development of Ultrabright Semiconducting Polymer Dots for Ratiometric pH Sensing

Yang-Hsiang Chan, **Changfeng Wu**, **Fangmao Ye**, **Yuhui Jin**, **Polina B. Smith**, and **Daniel T. Chiu***
Department of Chemistry, University of Washington, Seattle, Washington 98195

Abstract

Semiconducting polymer-based nanoparticles (Pdots) have recently emerged as a new class of ultrabright probes for biological detection and imaging. This paper describes the development of poly(2,5-di(3', 7'-dimethyloctyl)phenylene-1,4-ethynylene) (PPE) Pdots as a platform for designing Förster resonance energy transfer (FRET)-based ratiometric pH nanoprobes. We describe and compare three routes for coupling the pH-sensitive dye, fluorescein, to PPE Pdots, which is a pH-insensitive semiconducting polymer. This approach offers a rapid and robust sensor for pH determination using the ratiometric methodology where excitation at a single wavelength results in two emission peaks, one that is pH-sensitive and the other one pH-insensitive for use as an internal reference. The linear range for pH sensing of the fluorescein-coupled Pdots is between pH 5.0 to 8.0, which is suitable for most cellular studies. The pH-sensitive Pdots show excellent reversibility and stability in pH measurements. In this paper, we use them to measure the intracellular pH in HeLa cells following their uptake by endocytosis, thus demonstrating their utility for use in cellular and imaging experiments.

Keywords

ratiometric pH measurement; semiconducting polymer nanoparticles; FRET

Introduction

The ability to probe the spatiotemporal aspects of cellular signaling and communication is critical for understanding cellular function. Fluorescence microscopy, in combination with fluorescent probes and sensors, is now being widely used to study the organization and dynamics of single cells.[1–3] Fluorescent probes that report the state of important cellular parameters and second messengers, such as pH and calcium,[4–9] have been particularly useful for these experiments. For example, knowing the local pH within a sub-cellular organelle is a pre-requisite to understanding the physiological processes that take place in these small volumes because changes in pH can have a drastic effect on biomolecular structure and enzyme activity.[10, 11] We have been particularly interested in monitoring the pH inside single synaptic vesicles because the intra-vesicular pH is directly linked to the loading of neurotransmitters into these nanostructures.[12]

*Authors to whom correspondence should be addressed.

Supporting Information Available

We have included the following information: (1) emission spectra of PFPV Pdots and PFO-fluorescein pair; (2) emission spectra of different blending percentages of PS-SH/PS-NH_2 in the PPE polymer; (3) lifetime data of Pdot(A) and Pdot(B). (4) dynamic light scattering measurements of Pdots; (5) fluorescence spectra of bare PPE Pdots from pH 5 to 8. This material is available free of charge via the internet at http://pubs.acs.org.

NIH-PA Author Manuscript
NIH-PA Author Manuscript
NIH-PA Author Manuscript

NIH-PA Author Manuscript

NIH-PA Author Manuscript

NIH-PA Author Manuscript

The development of fluorescent indicators for intracellular pH has been reviewed recently by Han *et al*.[13] Among the various sensing schemes, there has been ongoing interest in exploiting nanoparticle-based probes as reliable fluorescent reporters. In comparison to fluorescent dyes, nanoparticle-based probes are much brighter because many dye molecules can be embedded inside a single nanoparticle. For example, Kopelman and coworkers have developed a series of nanoparticle-based sensors named PEBBLE where different types of fluorescent analyte-responsive indicators are either covalently bonded or physically trapped within the polymeric nanoparticle matrices (e.g. polyacrylamide) of 20–600 nm in diameter.[14–17] Because of their small size, these nanosensors can then be introduced into cells via different approaches, including pico-injection, particle bombardment delivery, or endocytosis. Similarly, Rosenzweig *et al*. reported the use of nanometer-sized, phospholipid-coated, polystyrene beads for intracellular pH measurements in murine macrophages where the lipobeads were absorbed via phagocytosis.[18, 19] These methods allow for the simultaneous analysis of a number of cells while maintaining cell viability.

In addition to high brightness, nanoparticle-encapsulated fluorescent probes provide a platform for incorporating more than two types of dyes (e.g. one pH-responsive indicator and one pH-insensitive dye for use as an internal reference) within a single matrix for achieving ratiometric fluorescence detection. Ratiometric measurement has the advantage that it is minimally affected by the fluctuation of the excitation source, probe concentration, photobleaching of probes, or any drifts in the instrument or the environment. As a result, there has been significant interest recently in employing silica nanoparticles as a matrix for ratiometric pH sensing.[20–24] However, for many of these nanoparticle pH sensors, the leaching of the embedded dyes from the matrices has been a concern.[24, 25]

All of the above-mentioned work has been based on using a central, non-fluorescent matrix, such as latex, polymer, or silica. The use of an optically inert matrix limits the potential brightness and optical functionality of the final nanoparticle probe. Until now, there has been a paucity of studies that explore the use of fluorescent nanoparticles (e.g. semiconducting quantum dots) as matrices in ratiometric, nanoparticle-based, pH detection.[26–29] In these studies, the pH-sensitive dyes are covalently linked to the surface of the quantum dot where FRET occurs from the quantum dot to the pH-responsive dyes (or vice versa) once the quantum dots (or dyes) are excited. The pH is determined based on the ratio of fluorescence intensity of the dyes and the quantum dot. However, the cytotoxicity,[30] the stochastic blinking phenomenon,[31, 32] the requirement of delicate surface passivation,[33] and the difficulties in tailoring the surfaces of quantum dots[34, 35] are concerns that have limited their biological applications. Therefore, a nanoparticle that offers both high brightness and biocompatibility is needed to meet the demands for ratiometric pH measurements in cellular studies.

We have recently reported on the surface functionalization and bioconjugation of semiconducting polymer dots,[36, 37] and showed that Pdot-bioconjugates are much brighter (e.g. ~ 30×) than Qdot-bioconjugates.[36] In addition to greater brightness, Pdots also show high photostability and fast radiative rates.[38–41] Here, we describe the first pH-sensitive probe based on ultrabright Pdots. These reversible and robust Pdot pH sensors have a linear pH sensing range between pH 5 and 8, where pH determination is based on ratiometric measurements. We demonstrate the applicability of pH-sensitive Pdots by measuring the pH in endocytic organelles of HeLa cells, and thus their potential for use in a wide range of cellular and imaging studies.

NIH-PA Author Manuscript

NIH-PA Author Manuscript

NIH-PA Author Manuscript

Results and Discussion

Our strategy was to create pH-sensitive Pdots that exploited highly efficient energy transfer from a pH-insensitive matrix of the Pdot to pH-sensitive dye molecules conjugated to the Pdot surface or matrix. Functionalization of Pdots was achieved by blending a general copolymer, such as poly(styrene-co-maleic anhydride) or thiol-terminated polystyrene, with the matrix of the semiconducting polymer during the preparation of Pdots thereby forming carboxyl-terminated or thiol-terminated groups that allowed for conjugation to the pH-sensitive dyes.

Selection and Optimization of Pdot-Dye Pair

We wanted to create a ratiometric, pH sensitive Pdot based on FRET that could be excited at a single wavelength with two different color emissions. The first step was to select a suitable donor-acceptor pair (see Supporting Information). Here, we found that PPE Pdots exhibited excellent energy transfer to fluorescein because of the substantial spectral overlap between the emission spectrum of PPE and the absorption spectrum of fluorescein (Figure 1A).

Conjugation of Fluorescein isothiocyanate (FITC) to PPE Pdots

Once we identified the best Pdot-fluorescein pair, we covalently linked the fluorescein molecules to the Pdot matrix. Here we introduce three routes to synthesize pH sensitive Pdots and the motivation for developing each will be described below.. Scheme 1 shows the three routes we characterized: For routes A and C, we first prepared the thiol-functionalized PPE Pdots by blending the thiol-terminated polystyrene into the PPE polymer, forming the PS-SH *co* PPE Pdots in aqueous solution with the nano-precipitation method. Subsequently, the PS-SH *co* PPE Pdots were reacted with FITC (route A) or fluorescein-5-maleimide (route C), generating the pH-sensitive Pdot-fluorescein complex.

To react with FITC, we also tried to employ amine-functionalized PPE Pdots. Unfortunately, we found amine-functionalized PPE Pdots were unstable and tended to self-aggregate in aqueous solution. To circumvent this problem, we devised route B where we first coupled FITC to amino-terminated polystyrene ($PS\text{-}NH_2$) in organic phase, after which we blended the fluorescein-functionalized PS with the PPE polymer during nano-precipitation and Pdot formation. We called the Pdot-fluorescein complex formed by routes A, B, and C, Pdot(A), Pdot(B), and Pdot(C), respectively.

The ratiometric sensing capability of each of the three systems was then systematically studied by varying the ratio of PPE polymer to PS-fluorescein. For routes A and C, we examined different blending percentages of PS-SH in the PPE polymer (Figure S2A) and found the optimal ratio to be 30% for PS-SH. For route B, best ratiometric pH sensing was observed when we used 60% of $PS\text{-}NH_2$-fluorescein (Figure S2B).

FRET between PPE and Fluorescein

For all three coupling routes, we observed highly efficient FRET from PPE to fluorescein (upper right inset in Figure 1A), which arises from the excellent spectral overlap between the emission spectrum of PPE (red solid line in Figure 1A) and the absorption spectrum of fluorescein (black dashed line in Figure 1A). For example, in the case of Pdot(A), we compared the fluorescence spectrum of bare PS-SH *co* PPE Pdots of the same concentration (without fluorescein, red solid line) with the spectrum for PPE-fluorescein Pdots; the increase in emission from fluorescein (λ = 513 nm, blue solid line) with concomitant suppression of PPE Pdot emission (λ = 420–490 nm, blue solid line) clearly indicated efficient FRET from PPE to fluorescein. We also note that emission intensity of free fluorescein at the same concentration was very weak when excited at the same wavelength

NIH-PA Author Manuscript

NIH-PA Author Manuscript

NIH-PA Author Manuscript

of 390 nm (green solid line, Figure 1A), which indicates emission from fluorescein was caused by energy transfer from PPE.

To further confirm FRET between PPE and fluorescein, we measured the time-resolved fluorescence decay curves of PS-SH *co* PPE Pdots without fluorescein and the PPE Pdot-fluorescein complex (Pdot(C); see Figure 1B). The fluorescence lifetime of PS-SH *co* PPE Pdots was 0.30 ns while the lifetime of Pdot(C) was shortened to 0.21 ns, which also supports the presence of FRET from PPE to fluorescein. The lifetimes of Pdot(A) and Pdot(B) are included in the supplementary materials (Figure S3).

The size of the final Pdot-fluorescein nanoparticle is important for biological applications. We determined the hydrodynamic diameters of the PPE Pdot-fluorescein by dynamic light scattering (DLS) as 26 nm, 25 nm, and 26 nm on average for Pdot(A), Pdot(B), and Pdot(C), respectively (Figure S4). Figure 1C and 1D shows a typical transmission electron microscopy (TEM) image of Pdot(C) and a histogram that plots the measured size distribution, which indicates an average diameter of 25 nm in agreement with our DLS measurements. We note the size of Pdots can be tuned,[38] from a few nanometers to hundreds of nanometers, depending on the requirements of the end application.

pH-Sensitivity and Reversibility Measurements

We characterized the pH sensitivity for all three systems (Pdot(A), Pdot(B), Pdot(C)). Figure 2 shows the emission peak of fluorescein increased with increasing pH (λ_{exc} = 390 nm) due to the deprotonation of its carboxylic acid and phenol moieties,[42] while the fluorescence intensity of PPE Pdots remained constant (λ_{exc} = 390 nm). We also examined the pH response of bare PPE Pdots without fluorescein (Figure S5), and confirmed that PPE Pdot is pH non-responsive from pH=5.0 to 8.0, thus rendering it as a good internal reference for ratiometric pH sensing.

Figure 3A shows that the ratio of the emission intensities of fluorescein (λ = 513 nm) to PPE (λ = 440 nm) changed linearly as a function of pH in the range of pH 5.0 to 8.0 for these three systems. Among them, Pdot(A) exhibited the highest detection sensitivity with I_{513nm}/I_{440nm} varying by 0.37 per unit change in pH. Despite this high pH sensitivity, we were concerned that the thiocarbamoyl unit between thiol and isothiocyanate would be prone to gradual degradation in the presence of excess free thiols,[43] thus potentially compromising the stability of Pdot(A) in more complicated biological applications. This concern motivated us to develop Pdot(B), which provides a stable amine-isothiocyanate adduct between the Pdot and fluorescein. The longer side chain of PS-NH_2 in Pdot(B), however, led to less efficient energy transfer and a corresponding lower pH sensitivity of 0.18 per unit change in pH. As a result, we also developed Pdot(C), which was aimed to offer a compromise between high pH sensitivity and bond stability. The ratio of I_{513nm}/I_{440nm} for Pdot(C) varied by 0.29 per unit change in pH.

We found all three Pdot sensors showed excellent reproducibility and reversibility in reporting pH. Figure 3B illustrates the reversibility of Pdot pH sensors in an experiment where we changed the pH of the solution containing Pdots repeatedly between pH 5 and pH 8. The reversibility and robustness of these Pdot pH sensors is evident from this experiment. Additionally, we note that the pH response time of the Pdot sensor was too fast for us to measure with a conventional fluorescence spectrometer. Fast pH response was expected because of the small size (i.e. large surface-to-volume ratio) of the Pdots and the rapid diffusion of protons.

NIH-PA Author Manuscript

NIH-PA Author Manuscript

NIH-PA Author Manuscript

Calculation of Förster Radius at Different pH

Because fluorescein absorbs energy mostly through FRET, it was important to investigate the FRET efficiency because it affects the pH sensing ability of Pdot-fluorescein. Here we take Pdot(C) as an example to illustrate the calculation of Förster radius at different pH. FRET is a non-radiative dipole-dipole interaction, and the efficiency of energy transfer (*E*) is given by:

$$E=\left[1+\left(\frac{r}{R_o}\right)^6\right]^{-1} \tag{1}$$

$$R_o{}^6=8.79\times10^{-5}(\kappa^2 n^{-4} Q_D J) \qquad (\text{in Å}) \tag{2}$$

where *r* is the distance between the donor and the acceptor, which is the distance between PPE and fluorescein, respectively, in our case. R_o is the Förster radius for which the energy transfer efficiency is diminished to 50% of the maximal value. κ is an orientation factor, which is set to 2/3 for a randomly orientated donor-acceptor pair in solution. *n* is the refractive index of the medium, which is 1.33 for water in our experiments. Q_D is the quantum yield of the donor in the absence of acceptors, which is 12% for PPE Pdots. *J* is the spectral integral as a function of wavelength, expressing the degree of spectral overlap between the emission spectrum of the donor and the absorption spectrum of the acceptor. To obtain the value of R_o, we had to calculate *J* first from the following equation:

$$J=\frac{\int_0^\infty F_D(\lambda)\varepsilon_A(\lambda)\lambda^4 d\lambda}{\int_0^\infty F_D(\lambda)d\lambda} \qquad (\text{in } \mathrm{M^{-1}cm^{-1}nm^4}) \tag{3}$$

where $F_D(\lambda)$ is the dimensionless emission intensity, λ is the wavelength, $\varepsilon_A(\lambda)$ is the pH-dependent molar absorption coefficient of the acceptor (fluorescein) at λ.

Figure 4A shows the degree of spectral overlap between the donor emission and the acceptor absorption at pH=5–8. Using this information, we calculated that the overlap integrals at pH=5 to 8 were all very close to ~1.1×10^{16} $\mathrm{M^{-1}cm^{-1}nm^4}$, which indicated the FRET efficiency of PPE to fluorescein remained fairly constant from pH 5 to 8. Figure 4B shows the corresponding Förster radius (R_o) to be ~5 nm. This result is in agreement with the fact that the PPE emission intensities (λ = 420–490 nm) of PPE-fluorescein complex remained constant under different pH conditions (Figure 2). Therefore, the increase in emission intensity of fluorescein from pH=5 to 8 can be ascribed to the increase in quantum yield of its deprotonated forms.[44]

Intracellular pH Measurements

To demonstrate the applicability of the ratiometric Pdot pH sensors, we introduced them into live HeLa cells via endocytosis without any additional reagents. After cellular uptake, we washed the cells with PBS buffer to remove free Pdots in solution and on the cell surface. Figure 5 shows the confocal fluorescence microscopy images of HeLa cells after the endocytosis of Pdots. Figure 5A–5D shows bare PPE Pdots without fluorescein, which served as our negative control. Figure 5E–5H shows Pdot(A); the blue channels (panels A

NIH-PA Author Manuscript

NIH-PA Author Manuscript

NIH-PA Author Manuscript

and E) were obtained by integrating the spectral region from 433–444 nm and green channels (panels B and F) were acquired by integrating the fluorescence signals from 507–518 nm. The intracellular pH was determined by comparing the ratio between the average fluorescence intensity from 507–518 nm and the average intensity from 433–444 nm to the pH calibration curve shown in Figure 3A. The average pH value based on at least 50 cells using the Pdot(A) system was determined to be 5.0 ± 0.7, which is in good agreement with the reported pH range for the acidic organelles involved in endocytosis, from pH ~6.5 in early endosomes to pH 4.5–5.0 in lysosomes.[45, 46]

The pH values measured by using the Pdot(B) and Pdot(C) probe were found to be 4.8 ± 0.9 and 4.9 ± 0.6, respectively (Figure 6). The relatively large standard deviations observed in the measured pH values reflect the wide pH differences in the various organelles of the endocytic pathway. Figure 6 top-right insets also show perfect co-localization of both PPE and fluorescein fluorescence, which indicates simultaneous uptake of PPE and fluorescein by HeLa cells and the fact PPE and fluorescein remained stably linked during the endocytic process. This experiment illustrates the potential application of pH-sensitive Pdots in cellular imaging experiments.

Conclusions

We report the design and performance of the first pH-sensitive Pdots that have ratiometric sensing capability with a linear pH sensing range (pH 5–8) suitable for most biological applications. The excellent pH sensitivity offered by these nanoparticles is derived from amplified energy transfer, which is characteristic of semiconducting polymers. Pdot-based pH sensors take advantage of many of the remarkable photophysical properties of Pdots, including their extraordinary brightness, excellent photostability, and easily tuned photophysical properties and physical dimensions. For example, this paper describes Pdot pH sensors that are about 25 nm in diameter but the dimensions of Pdots can be varied from a few nanometers to many tens of nanometers. We anticipate pH-sensitive Pdots to find broad use both in basic biological studies and in biomedical and clinical applications.

Experimental Section

Materials

The following chemicals were purchased from Sigma-Aldrich and used as received: 4-(2-Hydroxyethyl)piperazine-1-ethanesulfonic acid sodium salt, sodium hydroxide, poly(2,5-di(3',7'-dimethyloctyl)phenylene-1,4-ethynylene (PPE), tetrahydrofuran (THF; anhydrous, ≥ 99.9%, inhibitor-free), and hydrochloric acid. Poly(9,9-dioctylfluorenyl-2,7-diyl) (PFO), poly[{9,9-dioctyl-2,7-divinylene-fluorenylene}-alt-co-{2-methoxy-5-(2-ethylhexyloxy)-1,4-phenylene}] (PFPV), thiol-terminated polystyrene (PS-SH), amino-terminated polystyrene (PS-NH_2) were purchased from ADS Dyes, Inc. (Quebec, Canada) and used as received without further purification. All other chemical reagents were purchased from Invitrogen (Carlsbad, CA) and used as received. High purity water (18.2 MΩ•cm) was used throughout the experiment.

Preparation of Thiol-Functionalized PPE Pdots

40 μg of PPE and 12 μg of PS-SH were typically dissolved into 5 mL of THF. This mixture was then quickly injected into 10 mL of water under vigorous sonication. THF was then removed by purging with nitrogen on a 96 °C hotplate for one hour. The resulting Pdot solution was filtered through a 0.2 μm cellulose acetate membrane filter to remove any aggregates formed during preparation.

NIH-PA Author Manuscript

NIH-PA Author Manuscript

NIH-PA Author Manuscript

Preparation of Fluorescein-Conjugated PPE Pdots (Pdot(A), Pdot(B), and Pdot(C))

For Pdot(A), 0.2 mg of fluorescein isothiocyanate (FITC) dissolved in anhydrous DMSO was added to 4 mL of PS-SH *co* PPE Pdot (20 μg/mL) aqueous solution in a glass vial. The mixture was stirred for 12 h at room temperature and then was purified through a Bio-Rad Econo-Pac® 10DG column (Hercules, CA, USA) to separate the labeled Pdots from the free FITC molecules.

For the preparation of Pdot(B), 5 mg FITC and 20 mg PS-NH_2 were dissolved and mixed in 1 mL DMF. Then 5 mL triethylamine was added to the solution. The mixture was left on a rotary shaker overnight. 0.2 mL of PPE (1mg/1mL) in THF and 27 μL of the solution containing the PS-NH_2-FITC conjugate were mixed into 5 mL of THF. This mixture was then quickly injected into 10 mL of water under vigorous sonication. THF was then removed by purging with nitrogen on a 96 °C hotplate for one hour. The resulting Pdot(B) solution was first filtered through a 0.2 μm cellulose acetate membrane filter to remove any aggregates formed during preparation, and then purified through a Bio-Rad Econo-Pac® 10DG column.

For the preparation of Pdot(C), 15 μg of fluorescein-5-maleimide in anhydrous DMSO and 60 μL of concentrated 4-(2-hydroxyethyl)-1-piperazineethanesulfonic acid (HEPES) buffer (1 M) were added into a glass vial containing 4 mL of freshly prepared PS-SH *co* PPE Pdot (20 μg/mL) in aqueous solution. The mixture was stirred for 12 h at room temperature and was then purified through a Bio-Rad Econo-Pac® 10DG column.

Characterization of Pdots

The particle size was determined by dynamic light scattering (DLS) and transmission electron microscopy (TEM) to be 24–26 nm in diameter. For TEM, a drop of Pdot aqueous solution was placed on a carbon-coated grid and allowed to evaporate at room temperature. Electron micrographs of the synthesized Pdots were acquired using a FEI Tecnai F20 transmission electron microscope at an acceleration voltage of 200 kV.

The absorption spectra of Pdots were measured using UV-visible spectroscopy (DU 720, Beckman Coulter, Inc., CA USA). For the fluorescence measurements, 0.2 μg/mL of Pdots was prepared in 20 mM of HEPES buffer of various pH ranging from 5.0 to 8.0. The pH of the HEPES buffer solution was adjusted by the slow titration of 1 M NaOH or 1 N HCl. The fluorescence spectra were collected using a Fluorolog-3 fluorometer (HORIBA Jobin Yvon, NJ USA).

Cell Culture and Labeling

The cervical cancer cell line HeLa was ordered from American Type Culture Collection (ATCC, Manassas, VA, USA). Primary cultured HeLa cells were grown in Dulbecco's Modified Eagle Medium (cat. no. 11885, Invitrogen) supplemented with 10% Fetal Bovine Serum and 1% penicillin-streptomycin solution at 37 °C with 5% CO_2 humidified atmosphere. The cells were pre-cultured in a T-75 flask and allowed to grow for 5–7 days prior to experiments until ~80% confluence was reached. To prepare cell suspensions, the adherent cancer cells were quickly rinsed with media and then incubated in 5 mL trypsin-ethylenediaminetetraacetic (EDTA) solution (0.25 w/v % trypsin, 2.5 g/L EDTA) at 37°C for 5 min. The cell suspension solution was then centrifuged at 6000 rpm for 10 min to precipitate the cells in the bottom of the tube. After taking out the upper media, the cells was rinsed and re-suspended in 5 mL of culture media. Approximately tens of thousands HeLa cells were split onto a glass-bottomed culture dish and allowed to grow for 12 h before Pdot tagging. Prior to fluorescence imaging, the cells were rinsed with PBS buffer to remove any non-specifically attached Pdots on the cell surface.

NIH-PA Author Manuscript

NIH-PA Author Manuscript

NIH-PA Author Manuscript

Cell Imaging

The fluorescence spectra of Pdot-tagged cells were acquired with a fluorescence confocal microscope (Zeiss LSM 510) under ambient conditions (24 ± 2 °C). The confocal fluorescence images were collected using a diode laser at 405 nm (~15 mW) as the excitation source and an integration time of 1.6 μs/pixel. A Carl Zeiss 63× ("C-Apochromat" 63×/1.2 W Corr) objective was utilized for imaging and spectral data acquisition; the laser was focused to a spot size of ~5 μm^2.

Supplementary Material

Refer to Web version on PubMed Central for supplementary material.

Acknowledgments

DTC gratefully acknowledges support for this research from the National Institutes of Health (NS062725). We also acknowledge support from the Keck Imaging Center and Center for Nanotechnology at the University of Washington for use of instruments.

References

1. Rubinson EH, Gowda ASP, Spratt TE, Gold B, Eichman BF. Nature. 2010 ASAP.
2. Rosenfeld N, Young JW, Alon U, Swain PS, Elowitz MB. Science 2005;307:1962–1965. [PubMed: 15790856]
3. Kotecha N, Flores NJ, Irish JM, Simonds EF, Sakai DS, Archambeault S, Diaz-Flores E, Coram M, Shannon KM, Nolan GP, Loh ML. Cancer Cell 2005;14
4. Paredes RM, Etzler JC, Watts LT, Zheng W, Lechleiter JD. Methods 2008;46:143–151. [PubMed: 18929663]
5. Hornig S, Biskup C, Grafe A, Wotschadlo J, Liebert T, Mohr GJ, Heinze T. Soft Matter 2008;4:1169–1172.
6. Doussineau T, Smaihi M, Mohr GJ. Adv. Funct. Mater 2009;19:117–122.
7. Schulz A, Wotschadlo J, Heinze T, Mohr GJ. J. Mater. Chem 2010;20:1475–1482.
8. Burns A, Sengupta P, Zedayko T, Baird B, Wiesner U. Small 2006;2:723–726. [PubMed: 17193111]
9. Hilderbrand SA, Kelly KA, Niedre M, Weissleder R. Bioconjugate Chem. 2008
10. Demaurex N. News Physiol. Sci 2002;17:1–5. [PubMed: 11821527]
11. Boron, WF.; Boulpaep, EL. Medical Physiology. 2 ed.. Philadelphia: Elsevier Saunders; 2008.
12. Budzinski KL, Allen RW, Fujimoto BS, Kensel-Hammes P, Belnap DM, Bajjalieh SM, Chiu DT. Biophys. J 2009;97:2577–2584. [PubMed: 19883601]
13. Han J, Burgess K. Chem. Rev 2010;110:2709–2728. [PubMed: 19831417]
14. Clarka HA, Barkera SLR, Brasuela M, Millera MT, Monsona E, Parusa S, Shia Z-Y, Songa A, Thorsruda B, Kopelmana R, Adeb A, Meixnerb W, Atheyb B, Hoyerc M, Hillc D, Lightlec R, Philbert MA. Sens. Actuators B: Chem 1998;51:12–16.
15. Park EJ, Brasuel M, Behrend C, Philbert MA, Kopelman R. Anal. Chem 2003;75:3784–3791. [PubMed: 14572044]
16. Sun H, Scharff-Poulsen AM, Gu H, Almdal K. Chem. Mater 2006;18:3381–3384.
17. Lee Y-EK, Kopelman R. Nanomed. Nanobiotechnol 2009;1:98–110.
18. Ji J, Rosenzweig N, Griffin C, Rosenzweig Z. Anal. Chem 2000;72:3497–3503. [PubMed: 10952534]
19. McNamara KP, Nguyen T, Dumitrascu G, Ji J, Rosenzweig N, Rosenzweig Z. Anal. Chem 2001;73:3240–3246. [PubMed: 11476221]
20. Doussineau T, Trupp S, Mohr GJ. J. Colloid Interface Sci 2009;339:266–270. [PubMed: 19679316]
21. Gao F, Tang L, Dai L, Wang L. Spectrochim. Acta Part A 2007;67:517–521.

NIH-PA Author Manuscript

NIH-PA Author Manuscript

NIH-PA Author Manuscript

22. Burns A, Owb H, Wiesner U. Chem. Soc. Rev 2006;35:1028–1042. [PubMed: 17057833]
23. Lei J, Wang L, Zhang J. Chem. Commun 2010;46:8445–8447.
24. Peng J, He X, Wang K, Tan W, Wang Y, Liu Y. Anal. Bioanal. Chem 2007;388:645–654. [PubMed: 17440714]
25. Peng, H-s; Stolwijk, JA.; Sun, L-N.; Wegener, J.; Wolfbeis, OS. Angew.Chem. Int. Ed 2010;49:4246–4249.
26. Snee PT, Somers RC, Nair G, Zimmer JP, Bawendi MG, Nocera DG. J. Am. Chem. Soc 2006;128:13320–13321. [PubMed: 17031920]
27. Jin T, Sasaki A, Kinjob M, Miyazaki J. Chem. Commun 2010;46:2408–2410.
28. Chen Y, Thakar R, Snee PT. J. Am. Chem. Soc 2008;130:3744–3745. [PubMed: 18321112]
29. Suzuki M, Husimi Y, Komatsu H, Suzuki K, Douglas KT. J. Am. Chem. Soc 2008;130:5720–5725. [PubMed: 18393422]
30. Derfus AM, Chan WCW, Bhatia SN. Nano Lett 2004;4:11–18.
31. Yao J, Larson DR, Vishwasrao HD, Zipfel WR, Webb WW. Proc. Natl. Acad. Sci 2005;102:14284–14289. [PubMed: 16169907]
32. Medintz IL, Uyeda HT, Goldman ER, Mattoussi H. Nature Mater 2005;4:435–446. [PubMed: 15928695]
33. Liu Y-S, Sun Y, Vernier PT, Liang C-H, Chong SYC, Gundersen MA. J. Phys. Chem. C 2007;111:2872–2878.
34. Michalet X, Pinaud FF, Bentolila LA, Tsay JM, Doose S, Li JJ, Sundaresan G, Wu AM, Gambhir SS, Weiss S. Science 2005;307:538–544. [PubMed: 15681376]
35. Sapsford KE, Pons T, Medintz IL, Mattoussi H. Sensors 2006;6:925–953.
36. Wu C, Schneider T, Zeigler M, Yu J, Schiro PG, Burnham DR, McNeill JD, Chiu DT. J. Am. Chem. Soc 2010;132:15410–15417. [PubMed: 20929226]
37. Wu C, Jin Y, Schneider T, Burnham DR, Smith PB, Chiu DT. Angew. Chem. 2010 ASAP.
38. Wu C, Bull B, Szymanski C, Christensen K, McNeill J. ACS Nano 2008;2:2415–2423. [PubMed: 19206410]
39. Kaeser A, Schenning APHJ. Adv. Mater 2010;22:2985–2997. [PubMed: 20535737]
40. Pecher J, Mecking S. Chem. Rev 2010;110:6260–6279. [PubMed: 20684570]
41. Tian Z, Yu J, Wu C, Szymanski C, McNeill J. Nanoscale 2010;2:1999–2011. [PubMed: 20697652]
42. Sjöback R, Nygren J, Kubista M. Spectrochim. Acta Part A 1995;51:L7–L21.
43. Conaway CC, Krzeminski J, Amin S, Chung F-L. Chem. Res. Toxicol 2001;14:1170–1176. [PubMed: 11559030]
44. Martin MM, Lindqvist L. J. Lumin 1975;10:381–390.
45. Vieira OV, Botelho RJ, Grinstein S. Biochem. J 2002;366:689–704. [PubMed: 12061891]
46. Bayer N, Schober D, Prchla E, Murphy RF, Blaas D, Fuchs R. J. Virol 1998;72:9645–9655. [PubMed: 9811698]

NIH-PA Author Manuscript
NIH-PA Author Manuscript
NIH-PA Author Manuscript

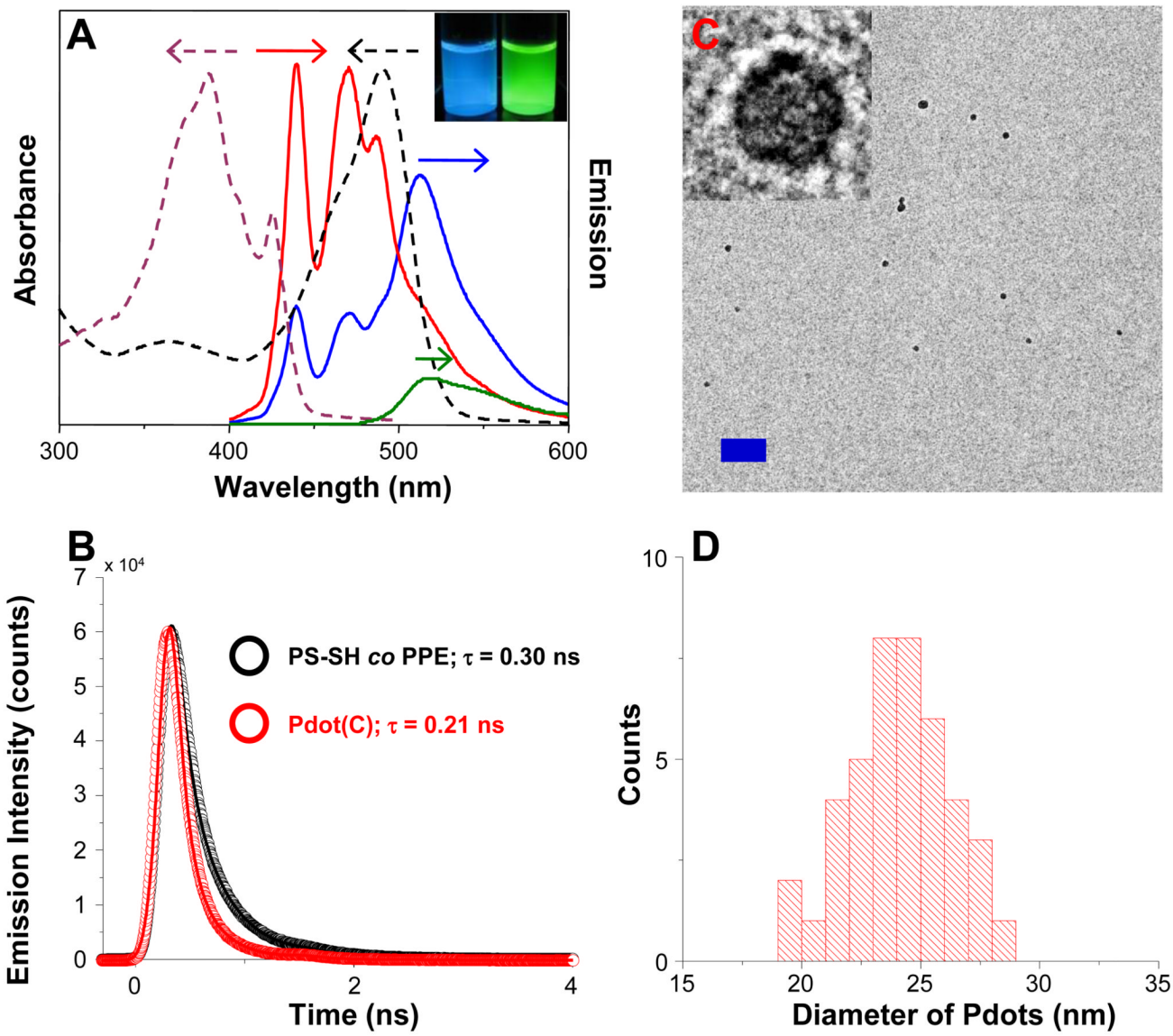

Figure 1.

Characterization of fluorescein-functionalized Pdots. (A) UV-visible spectra of PPE Pdots (dashed plum line) and FITC (dashed black line) in water; emission spectra of PS-SH *co* PPE (solid red line), Pdot(A) Pdots (solid blue line), and FITC (solid green line) in pH 7 HEPES buffer when excited at 390 nm. The inset in the upper-right corner shows the photographs of solutions containing PS-SH *co* PPE (left) and Pdot(A) Pdot (right) under a 365 nm UV lamp. (B) Time resolved fluorescence decay of Pdots before (i.e. bare PS-SH *co* PPE Pdots; black circles) and after conjugation to fluorescein (i.e. Pdot(C); red circles) in pure water. (C) TEM image of Pdot(C) Pdots. The inset in the upper-left corner shows the enlarged view of a single Pdot(C). Scale bar represents 200 nm. (D) Size distribution of Pdot(C) Pdots as measured by TEM.

NIH-PA Author Manuscript

NIH-PA Author Manuscript

NIH-PA Author Manuscript

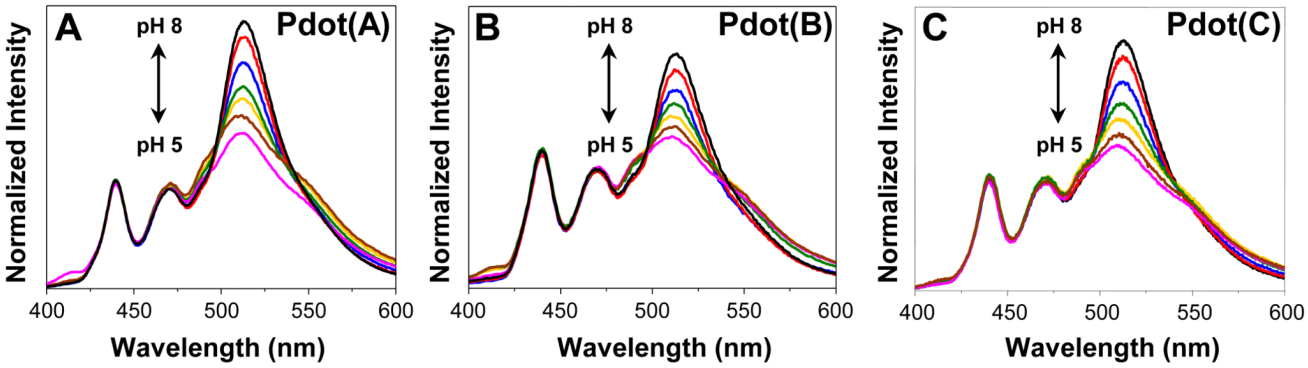

Figure 2.

Fluorescence spectra of (A) Pdot(A), (B) Pdot(B), and (C) Pdot(C) at different pH, ranging from 5 to 8 (black line: pH=8, red line: pH=7.5, blue line: pH=7, green line: pH=6.5, gold line: pH=6, brown line: pH=5.5, pink line: pH=5). Excitation wavelength was 390 nm.

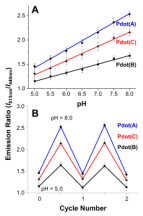

Figure 3.

pH sensitivity and reversibility of the three fluorescein-conjugated Pdots. (A) Ratiometric pH calibration plot of the emission ratio (I_{513nm}/I_{440nm}) of Pdot(A) (●), Pdot(B) (■), and Pdot(C) (▲) as a function of pH. The blue, black, and red lines are linear fit to the data of Pdot(A) (R^2 = 0.995), Pdot(B) (R^2 = 0.991), and Pdot(C) (R^2 = 0.994), respectively. The slopes for Pdot(A), Pdot(B), and Pdot(C) are 0.37, 0.18, and 0.29, respectively. (B) The intensity ratios (I_{513nm}/I_{440nm}) of Pdot(A) (●), Pdot(B) (■), and Pdot(C) (▲) when the pH was toggled between 5.0 and 8.0 repeatedly, illustrating the reversibility and reproducibility of pH sensing.

NIH-PA Author Manuscript NIH-PA Author Manuscript NIH-PA Author Manuscript

NIH-PA Author Manuscript

NIH-PA Author Manuscript

NIH-PA Author Manuscript

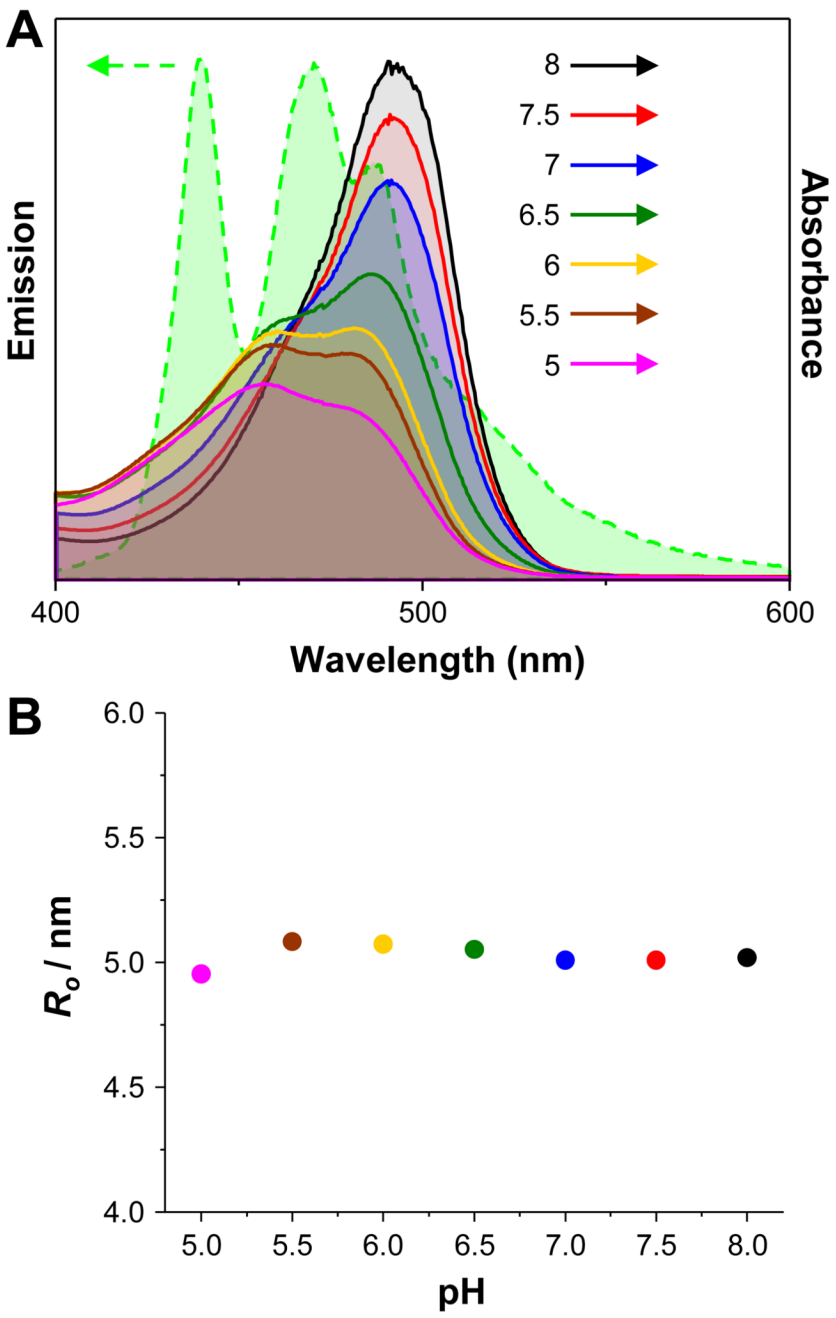

Figure 4.

Illustration of spectral overlap between the emission of donor (i.e. PPE) and the absorption of acceptor (i.e. FITC), and their calculated Förster distance, R_o. (A) Emission spectrum of PS-SH-FITC *co* PPE Pdots (dashed light green line) and excitation spectra of FITC at pH ranging from 5 to 8. The areas under the curves were colored for easier visualization of spectral overlap. (B) The corresponding Förster distance of PPE-FITC at different pH was plotted based on the overlap integral shown in (A).

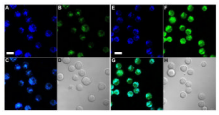

Figure 5.

Confocal microscopy images of HeLa cells labeled by (A–C) pure PPE Pdots and (E–G) Pdot(A) at λ_{exc} = 405 nm; their corresponding bright-field images are shown in (D) and (H), respectively. The blue fluorescence shown in (A) and (E) was produced by integrating the spectral region from 433–444 nm, while the green fluorescence shown in (B) and (F) was from 507–518 nm. The images (C) and (G) are the overlay of the blue and green fluorescence. The scale bars are 20 μm.

NIH-PA Author Manuscript
NIH-PA Author Manuscript
NIH-PA Author Manuscript

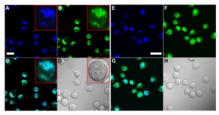

Figure 6.

Confocal microscopy images of HeLa cells labeled by (A–C) Pdot(B) and (E–G) Pdot(C) at λ_{exc} = 405 nm; their corresponding bright-field images are shown in (D) and (H), respectively. The blue channel shown in (A) and (E) was produced by integrating the spectral region from 433–444 nm, while the green channel shown in (B) and (F) was from 507–518 nm. The images in (C) and (G) are the overlay of the blue and green channels. The insets show a magnified view of a single HeLa cell. The scale bars are 20 μm.

NIH-PA Author Manuscript
NIH-PA Author Manuscript
NIH-PA Author Manuscript

NIH-PA Author Manuscript
NIH-PA Author Manuscript
NIH-PA Author Manuscript

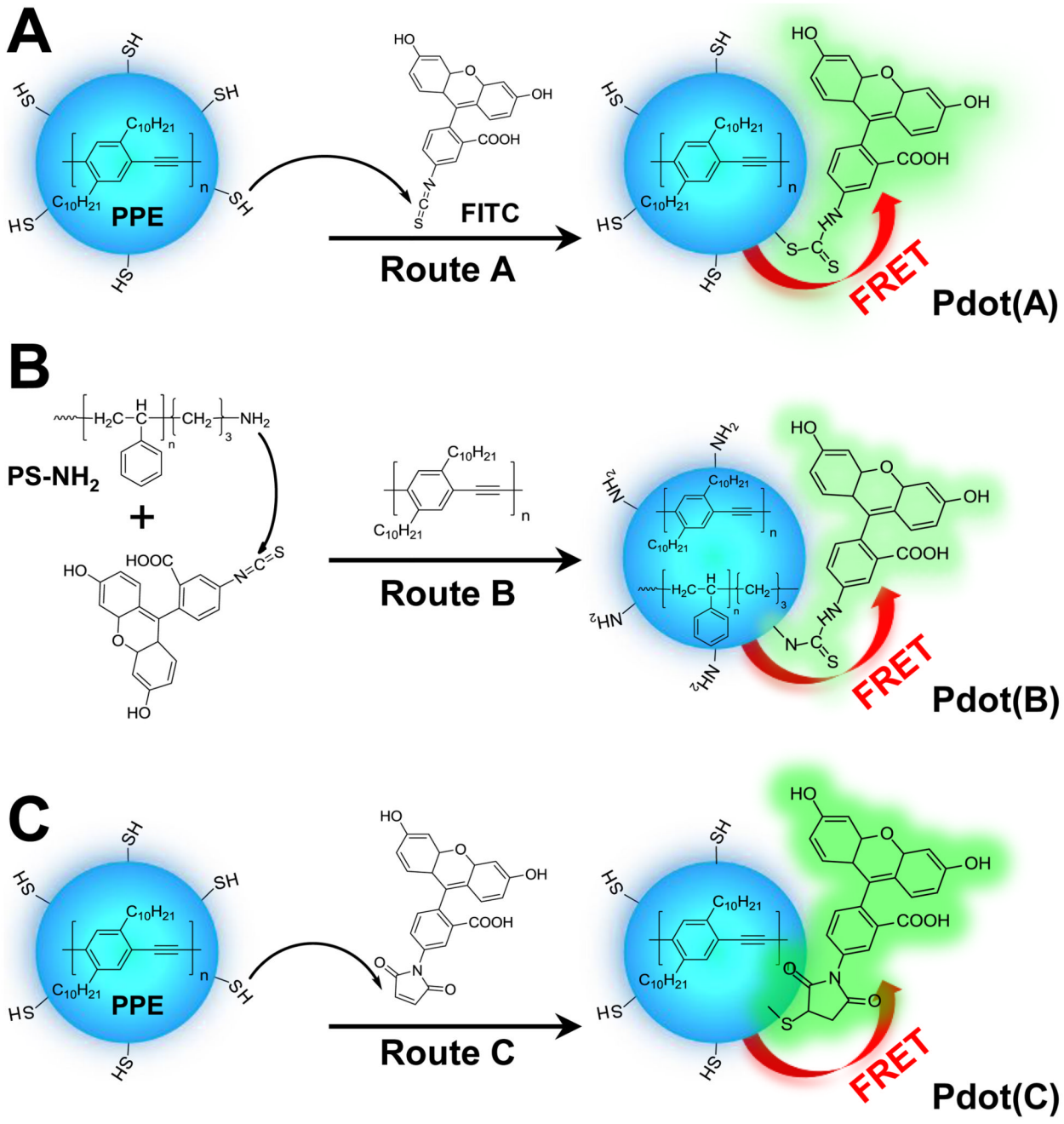

Scheme 1.

Schematic showing three routes for the preparation of PPE Pdot-based pH sensors. (A) PS-SH *co* PPE Pdots in water were first prepared and then reacted with the isothiocyanate moieties on the FITC molecules. (B) FITC was first conjugated to PS-NH_2 polymers through the amine-isothiocyanate reaction, and the resulting fluorescein-labeled PS polymers were blended with PPE polymers to form the PS-NH_2-FITC *co* PPE Pdots. (C) PS-SH *co* PPE Pdots were first prepared in the same way as (A), but were subsequently coupled to fluorescein-5-maleimide. PPE: poly(2,5-di(3',7'-dimethyloctyl)phenylene-1,4-ethynylene; PS: polystyrene polymer; FITC: fluorescein isothiocyanate.